5.4 STANDARD DEVIATION OF PHYSICAL PROPERTIES

Four additional sinter pot tests were carried out using the test procedure described in this report. The sinter mixture was the same as the mixture used in this project. The physical properties of the sinter produced in each sinter pot test were determined with the tumbler test (ISO 3271). The standard deviation of the results was calculated and is shown in **Table 7**. The results clearly show that the test procedure and results are repeatable.

Table 7: Standard deviation of tumbler index

Tumbler test results	A	B	C	D	Average	Standard deviation
TI %+6.30mm	70.38	71.17	70.74	70.81	70.78	0.32
TI %-6.30+0.50mm	25.06	24.36	24.92	24.93	24.82	0.31
AI %-0.50mm	4.56	4.46	4.34	4.26	4.41	0.13

5.5 PHASE COMPOSITION

Samples from each layer were prepared for chemical analyses (ICP) and the results are shown in **APPENDIX B**.

Samples were taken from each layer ensuring that the samples represent the sinter in that specific layer. Each representative sample was mounted in epoxy resin and then vacuum impregnated. The samples were polished to expose a plane section. After polishing, the samples were examined under an optical microscope. The volume proportions of phases in the sinter were estimated by using the point counting method. Around 1000 points were counted for the whole polished surface of the sample. The standard deviation of the results obtained by this method is ±0.5%. Results are shown in **APPENDIX C**.

With an energy dispersive microanalyser (EDA) attached to the scanning electron microscope (SEM) it was possible to obtain a quantitative analysis of each phase. The results of the quantitative analysis of each phase were used to calculate the

stoichiometry of each phase. Microphotographs were taken to illustrate the phases and their occurrence in the sinter samples.

5.5.1 HEMATITE

Three types of hematite commonly occur in this sinter. Massive hematite particles resemble the original hematite particles added to the raw materials mixture. These particles were only partially affected during sintering. Some of the massive hematite particles display recrystallised outer rims. In all the layers massive hematite dominates as the hematite phase. More than 75% of the hematite consists of massive hematite. An example of the microstructure containing massive hematite is shown in **Figure 11**.

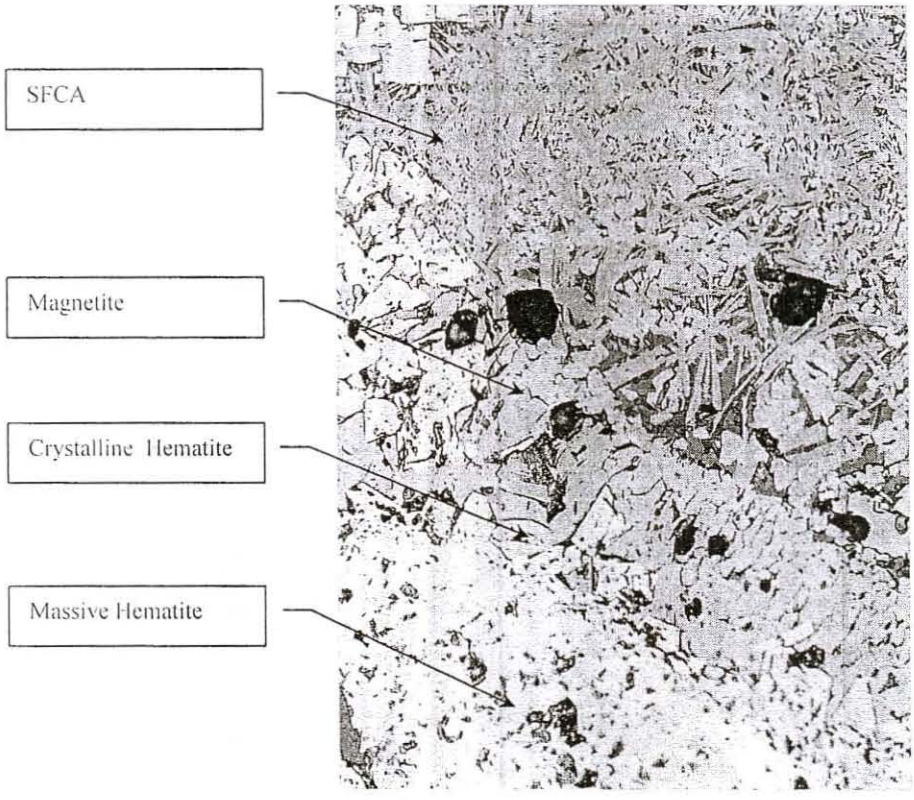

***Figure 11**: Massive hematite displaying a recrystallised rim of crystalline hematite. The hematite is associated with euhedral to subhedral magnetite crystals embedded in a silicate-rich glassy matrix (X 200).*

Magnetite follows the crystalline hematite at the periphery of the massive hematite particles (**Figure 11**). The crystalline hematite occurs as euhedral to subhedral as well

as skeletal and/or dendritic hematite crystals, which crystallise during cooling of the sinter. Approximately 20% of the hematite produced is crystalline hematite that precipitated from the melt.

The remaining hematite consists of very small quantities of secondary hematite. Secondary hematite is in general relatively scarce and probably crystallised due to re-oxidation of magnetite at high temperatures. Secondary hematite is usually bound in a matrix of calcium silicate and SFCA.

The hematite content of the sinter in series one decreased from the top layer to the bottom layer while the hematite content in the sinter in series two reached a maximum in the middle and decreased slightly in the bottom layer (**Figure 12**). The hematite content of series one (1100mmH_2O) is lower than the hematite content of series two (1500mmH_2O). The hematite content correlates with the magnetite content. The higher the magnetite content is, the lower is the hematite content.

Figure 12: Volume percentage of hematite

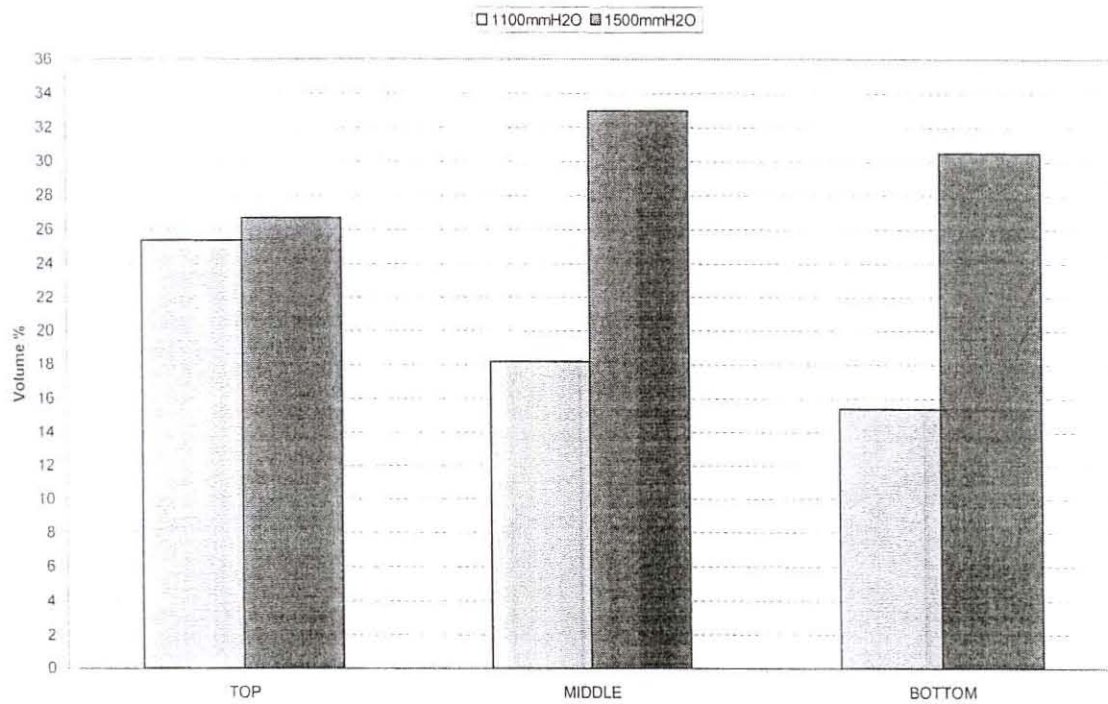

The chemical composition of hematite is shown in **Table 8**. The recalculation to determine the $\%Fe_2O_3$ is shown in **APPENDIX G**. The chemical composition of the hematite present in each layer is almost the same for both series of sinter pot tests as is evident from **Table 8**. A hypothesis test was conducted (**APPENDIX D**) to determine the relation between the chemical composition of the hematite in the different sinter layers. The hypothesis test indicated that there is no difference in the mean Fe_2O_3 content of the different layers.

Table 8: Chemical analyses of hematite

	Series1: 1100mmH_2O			Series 2: 1500mmH_2O		
	Top	**Middle**	**Bottom**	**Top**	**Middle**	**Bottom**
Fe_2O_3	96.81	95.42	96.66	97.03	95.71	95.35
FeO	0.00	0.00	0.00	0.00	0.00	0.00
SiO_2	0.12	0.01	0.07	0.16	0.83	0.37
TiO_2	0.10	0.26	0.18	0.17	0.04	0.09
CaO	0.26	0.30	0.31	0.19	0.71	0.53
SO_3	0.00	0.00	0.00	0.00	0.00	0.00
MnO	0.34	0.12	0.31	0.06	0.12	0.15
K_2O	0.01	0.00	0.00	0.01	0.00	0.00
MgO	0.14	0.01	0.01	0.01	0.07	0.01
Al_2O_3	0.88	1.54	0.59	0.53	0.33	1.07
Na_2O	0.01	0.00	0.01	0.00	0.01	0.00
P_2O_5	0.00	0.00	0.00	0.02	0.01	0.01

5.5.2 MAGNETITE

Magnetite could form during crystallisation from the melt or solid state reduction of hematite or solid state oxidation of wustite[13]. The magnetite is present as well defined euhedral to sub-hedral crystals as well as skeletal and dendritic crystals. Magnetite crystals are present in close association with SFCA, as shown in **Figure 13**.

The magnetite content in the middle and bottom layer of series one is higher than the magnetite content in the middle and bottom layer of series two (**Figure 14**). There is not a significant difference between the magnetite content in the top layers of both series.

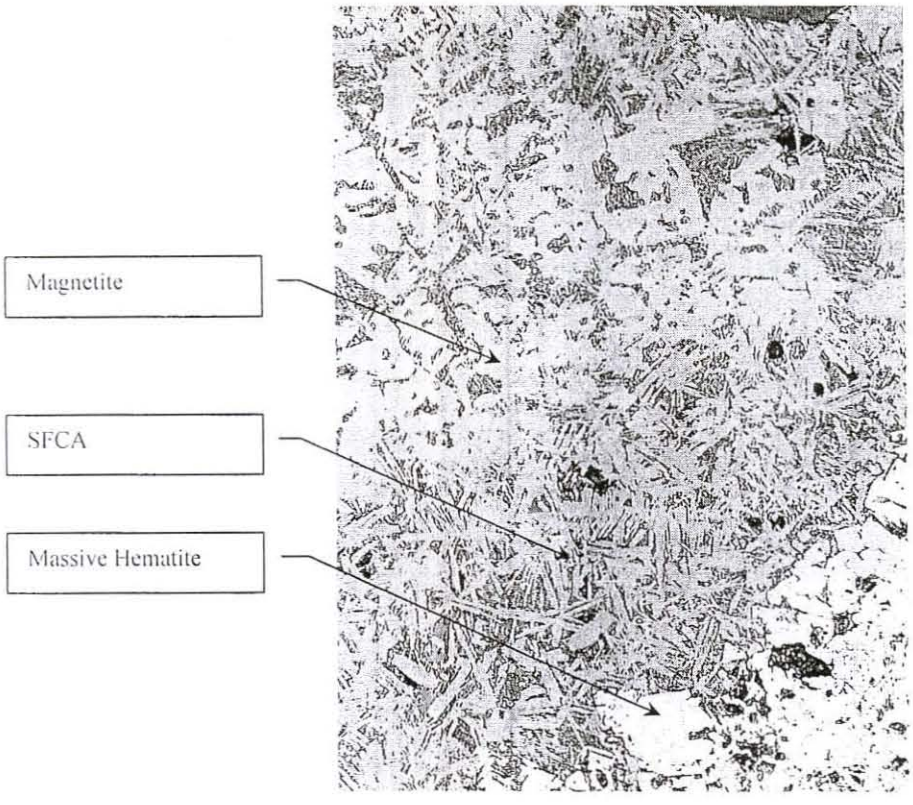

Figure 13: Magnetite crystals embedded in a silicate-rich glassy matrix. The magnetite is in close association with SFCA crystals (X 200).

Figure 14: Volume percentage of magnetite

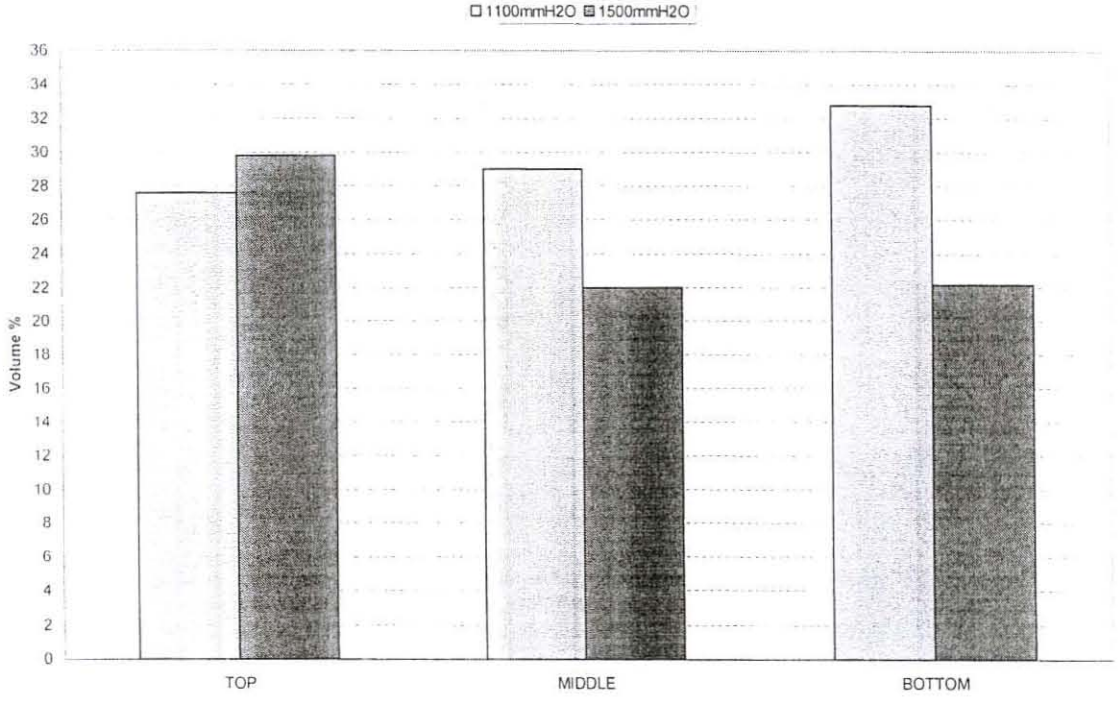

At a low airflow rate the sintering time at temperatures above 1100°C is longer. During sintering the surface of the hematite particle is reduced to magnetite. Due to the longer reaction time, more hematite is reduced to magnetite in series one than in series two.

Magnetite is also formed from the dissociation of SFCA at temperatures higher than 1300°C[(2)(4)]. The proportion of SFCA that is decomposed may increase when the time of exposure above the decomposition temperature increases or when the maximum temperature that is reached during sintering increases. Due to the longer time above 1300°C more magnetite was formed in series one than in series two.

The chemical composition of magnetite is shown in **Table 9**. The recalculation to determine the $\%Fe_2O_3$ and %FeO is shown in **APPENDIX G**. The chemical composition (**Table 9**) of the magnetite in the different layers is almost the same in both series of sinter pot tests.

Table 9: Chemical analyses of the magnetite

	Series1: 1100mmH_2O			Series 2: 1500mmH_2O		
	Top	**Middle**	**Bottom**	**Top**	**Middle**	**Bottom**
Fe_2O_3	69.20	67.71	69.31	67.59	68.06	68.51
FeO	19.10	21.57	20.35	23.29	19.83	19.11
SiO_2	0.02	0.08	0.05	0.12	0.10	0.03
TiO_2	0.01	0.04	0.02	0.04	0.02	0.02
CaO	2.07	1.86	2.04	2.39	2.11	2.42
SO_3	0.00	0.00	0.00	0.00	0.00	0.00
MnO	1.73	1.48	1.86	1.16	2.73	1.72
K_2O	0.00	0.00	0.00	0.00	0.00	0.00
MgO	4.74	3.50	4.08	2.37	3.56	4.42
Al_2O_3	1.22	1.54	1.27	1.58	1.21	1.44
Na_2O	0.00	0.00	0.01	0.00	0.01	0.01
P_2O_5	0.00	0.00	0.00	0.01	0.01	0.00

Figure 15 and **Figure 16** shows the mass percentage (Fe_2O_3 + Al_2O_3) versus the mass percentage (FeO + MgO + CaO + MnO). The well-grouped data as shown by **Figure 15** and **Figure 16** indicate that the chemical composition of the magnetite in the different layers is almost the same. A hypothesis test was conducted (**APPENDIX E**) to determine the relation between the chemical composition of the magnetite in the

different sinter layers. The hypothesis test indicated that there is no difference in the chemical composition of the different layers.

Figure 15: Magnetite (Series 1)

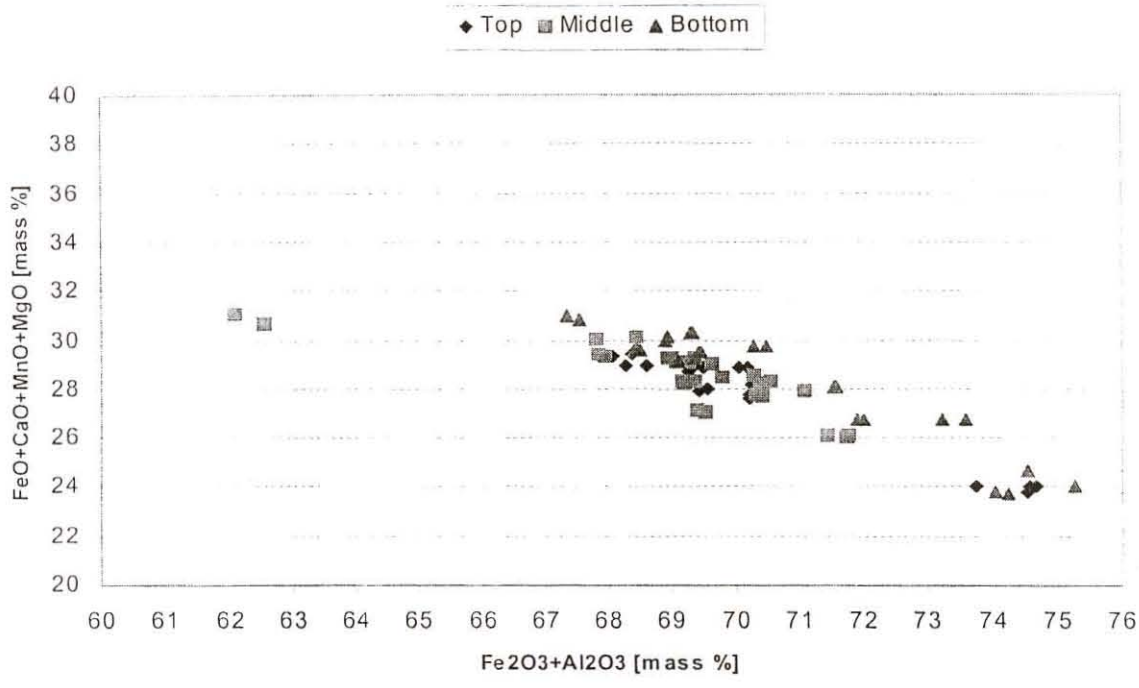

Figure 16: Magnetite (Series 2)

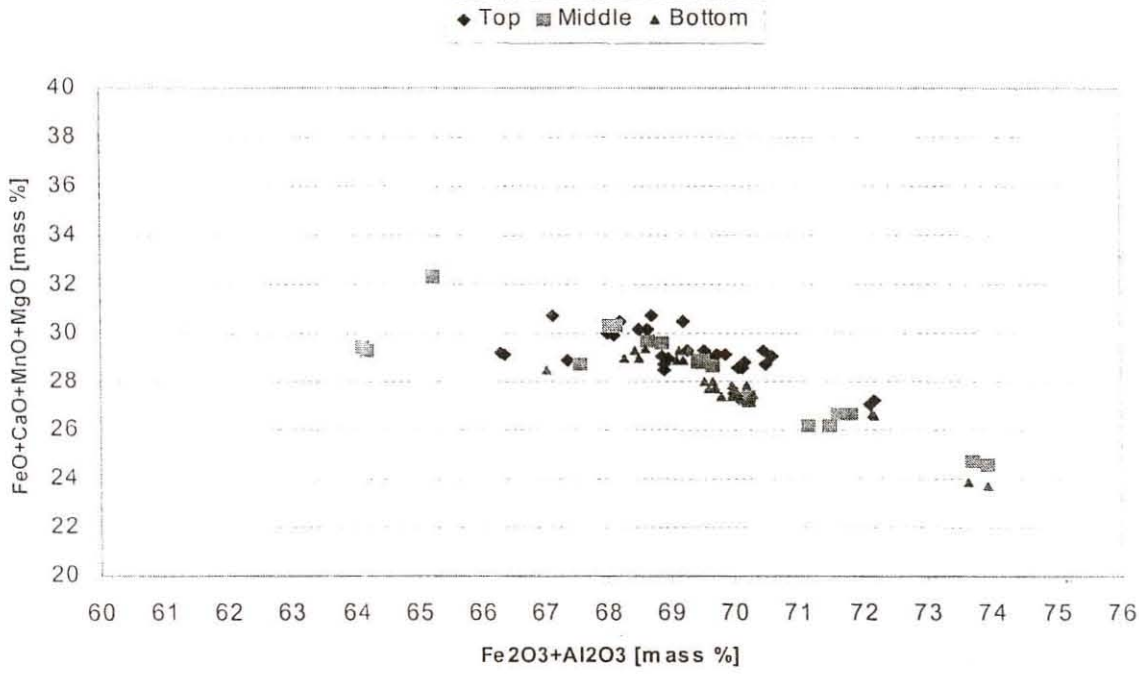

The calculated stoichiometry (**Table 10**) of the magnetite in all the layers agrees very well with the generally accepted formula for magnetite. The generally accepted formula for magnetite is XY_2O_4 = $(Fe,Mg,Si,Ca,Mn)(Fe,Al)_2O_4$. An example to show how the stoichiometry was calculated is shown in **APPENDIX G**.

Table 10: Stoichiometry of the magnetite

XY_2O_4 = $(Fe,Mg,Si,Ca,Mn)(Fe,Al)_2O_4$

	Series1: 1100mmH_2O			Series 2: 1500mmH_2O		
	Top	**Middle**	**Bottom**	**Top**	**Middle**	**Bottom**
Fe^{2+}	0.60	0.68	0.64	0.74	0.63	0.60
Mg^{2+}	0.26	0.20	0.22	0.13	0.20	0.25
Si^{4+}	0.00	0.00	0.00	0.00	0.00	0.00
Ca^{2+}	0.08	0.07	0.08	0.10	0.08	0.10
Mn^{2+}	0.05	0.05	0.06	0.04	0.09	0.05
X	**1.00**	**1.01**	**1.00**	**1.01**	**1.01**	**1.00**
Fe^{3+}	1.95	1.92	1.94	1.92	1.94	1.93
Al^{3+}	0.05	0.07	0.06	0.07	0.05	0.06
Y	**2.00**	**1.99**	**2.00**	**1.99**	**1.99**	**2.00**
O^{2-}	**4.00**	**4.00**	**4.00**	**4.00**	**4.00**	**4.00**

5.5.3 SFCA

SFCA usually contains SiO_2 and Al_2O_3 and is referred to as silico-ferrites of calcium and aluminium (SFCA). SFCA are present as dendritic SFCA, acicular SFCA and tabular SFCA according to the size of the crystals.

Dendritic SFCA is the first type of SFCA formed during the sintering process[9]. Dendritic crystals are very small, usually smaller than 4μm (**Figure 17**). Approximately 15% of the total SFCA consist of dendritic SFCA.

Crystal growth between 1200°C and 1300°C results in bigger crystals, bigger than 4μm but smaller than 10μm, called acicular SFCA[9] as shown in **Figure 18**. Acicular SFCA dominates as the SFCA phase in all the layers. More than 75% of the total SFCA consists of acicular SFCA.

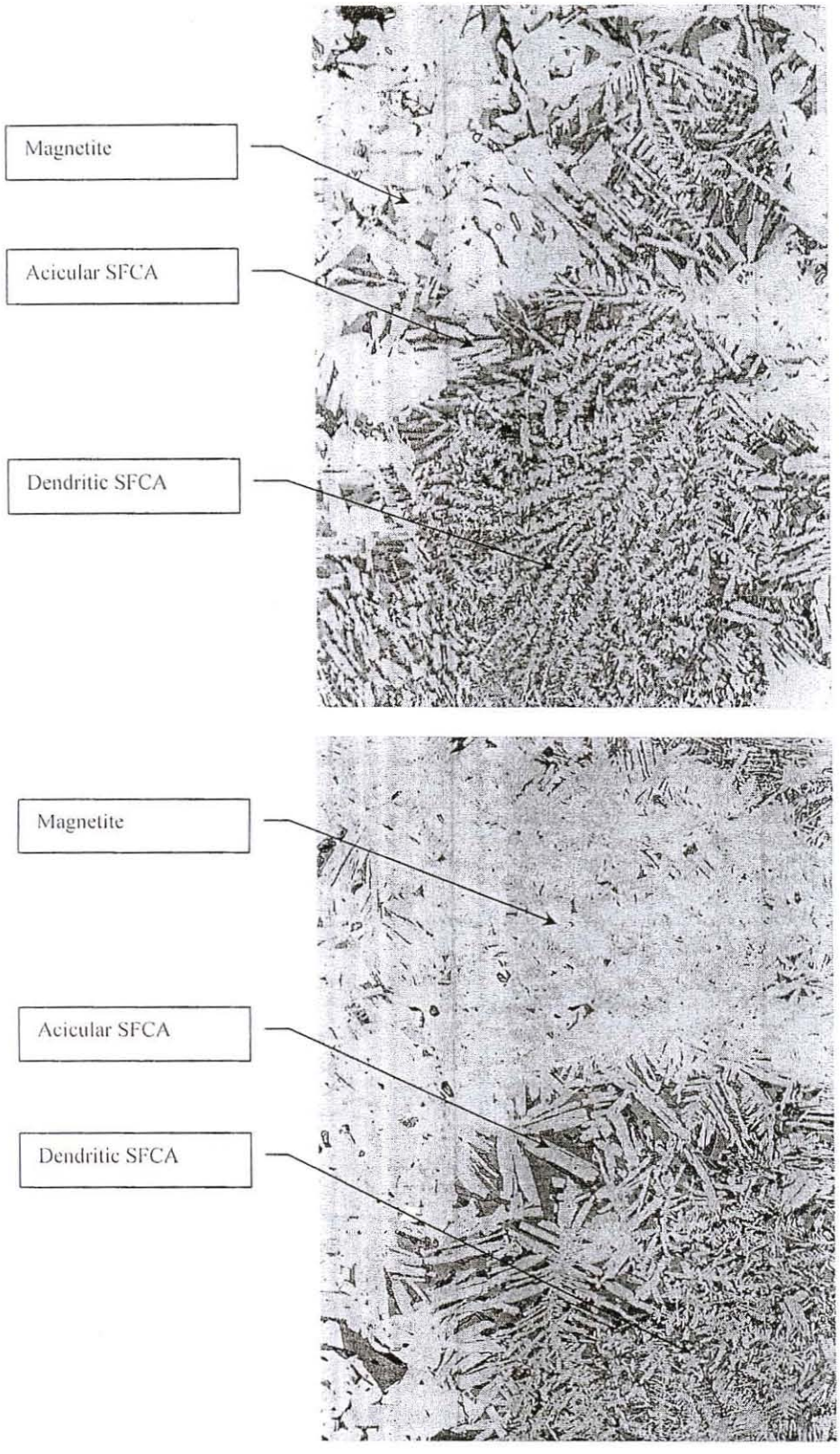

***Figures 17 and 18**: Dendritic SFCA is the first type of SFCA formed during the sintering process. Crystal growth results in bigger crystals called acicular SFCA (X 200).*

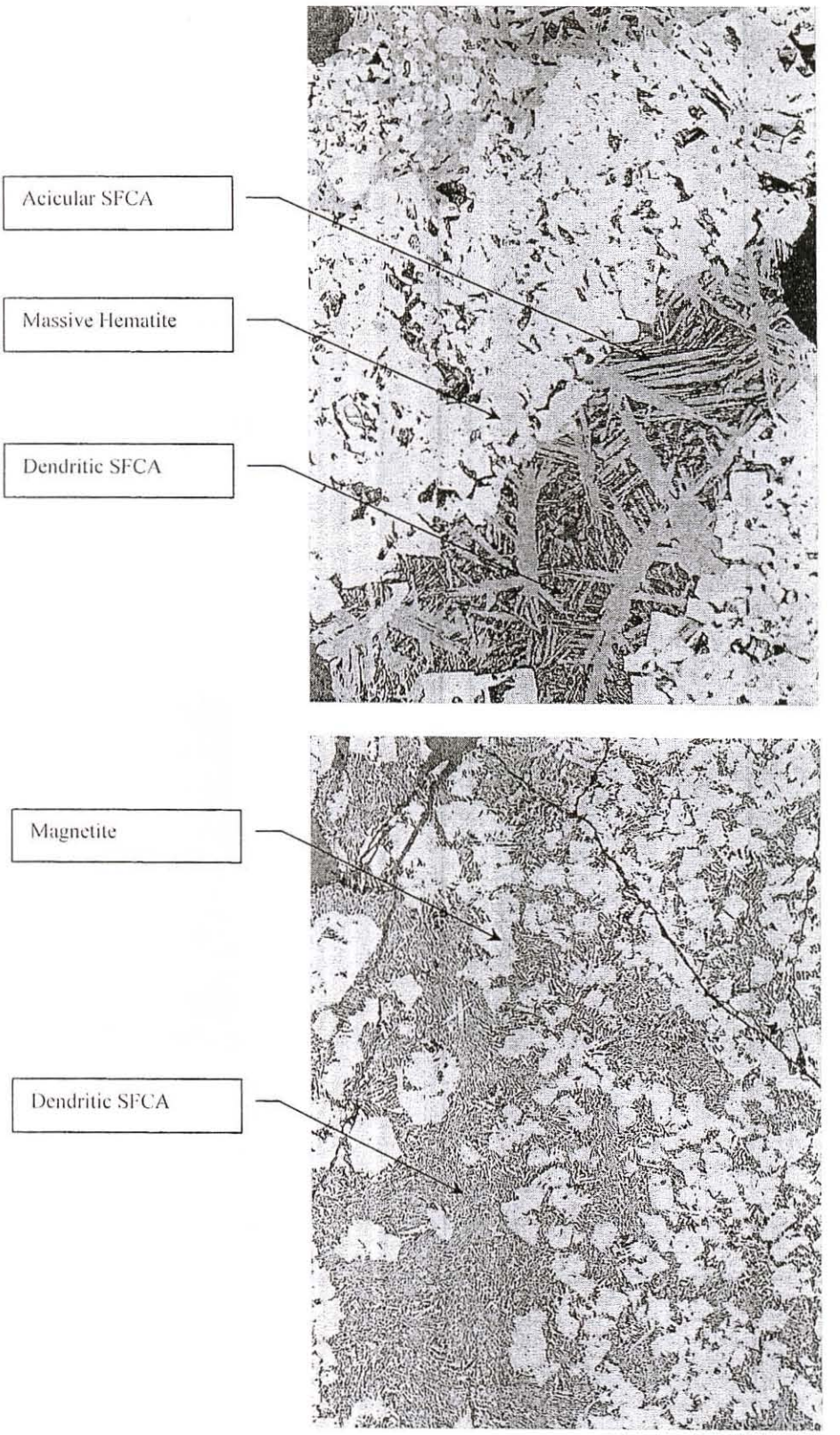

***Figures 19 and 20**: SFCA in association with massive hematite and SFCA in association with magnetite (X 200).*

At 1300°C acicular SFCA melts and precipitates as columnar SFCA during cooling. These are rather large crystals with a typical size of 10μm and bigger[9]. Approximately 10% of the total SFCA consist of columnar SFCA.

In series one the highest SFCA content is found to be in the middle layer and the lowest in the top layer. In series two the total SFCA content increased from the top layer to the bottom layer (**Figure 21**). The total SFCA content of series one is higher than the total SFCA content of series two.

Figure 21: Volume percentage of SFCA

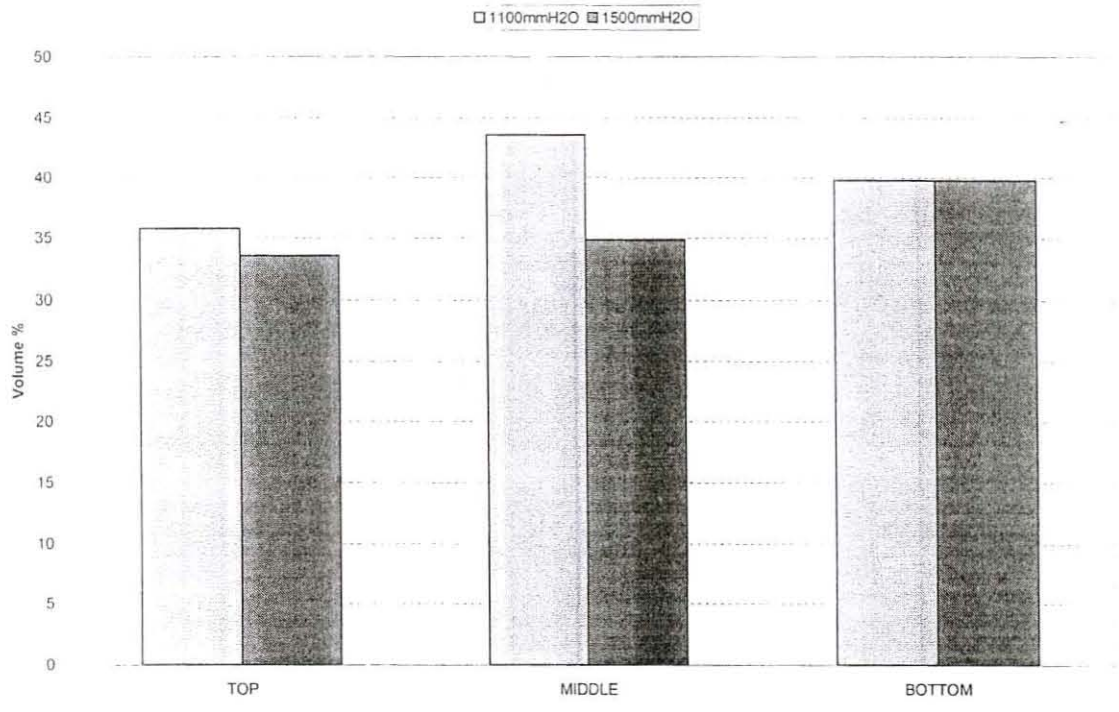

SFCA is the product of several successive reactions[14]:

1. The formation of monocalcium ferrite at temperatures from 1050°C to 1150°C.
2. The reaction between Al_2O_3 and CaO to produce calcium aluminate (1100°C-1150°C).
3. Dissolution of the calcium aluminate in monocalcium ferrite at 1100°C-1150°C to produce aluminous monocalcium ferrite.
4. Fusion of the aluminous monocalcium ferrite and reaction with Fe_2O_3 at 1200°C-1250°C to produce aluminous hemicalcium ferrite.
5. Reaction with SiO_2 at 1200°C-1250°C to produce SFCA.

From the above it is clear that the formation of SFCA will be enhanced by a longer time at temperatures above 1100°C. At a low airflow rate the sintering time at temperatures above 1100°C is longer. Therefore, the higher SFCA content in series one. The sintering time at temperatures above 1100°C increased from the top layer to the bottom layer resulting in a higher SFCA content in the middle and bottom layers.

The SFCA will begin to decompose when the temperature exceeds 1300°C[2][4]. At decomposition it will change to hematite when the partial pressure of oxygen is high and the temperature is lower than 1350°C. It will change to magnetite when the partial pressure of oxygen is low and the temperature is higher than 1350°C[2]. The proportion of SFCA that is decomposed may increase when the time of exposure above the decomposition temperature increases or when the maximum temperature that is reached during sintering increases. Therefore, it is important to control the maximum sintering temperature below 1300°C to prevent decomposition of SFCA.

The chemical composition of SFCA is shown in **Table 11**. The recalculation to determine the $\%Fe_2O_3$ and %FeO is shown in **APPENDIX G**. The chemical composition (**Table 11**) of the SFCA in the different layers is almost the same in both series of sinter pot tests.

Table 11: Chemical analyses of SFCA

	Series1: 1100mmH_2O			**Series 2: 1500mmH_2O**		
	Top	**Middle**	**Bottom**	**Top**	**Middle**	**Bottom**
Fe_2O_3	75.89	73.42	73.95	77.10	77.03	78.58
FeO	0.00	0.00	0.00	0.00	0.00	0.00
SiO_2	6.01	6.63	6.44	5.04	4.94	4.69
TiO_2	0.22	0.16	0.21	0.14	0.13	0.12
CaO	14.98	14.72	14.57	14.05	13.23	12.61
SO_3	0.00	0.00	0.00	0.02	0.00	0.02
MnO	0.56	0.51	0.72	0.58	1.36	0.89
K_2O	0.01	0.00	0.00	0.03	0.00	0.02
MgO	1.06	0.80	0.87	0.83	1.02	1.88
Al_2O_3	3.46	4.16	4.88	3.99	3.95	3.60
Na_2O	0.01	0.01	0.01	0.02	0.01	0.02
P_2O_5	0.02	0.00	0.01	0.19	0.02	0.03

Figure 22: SFCA (Series 1)

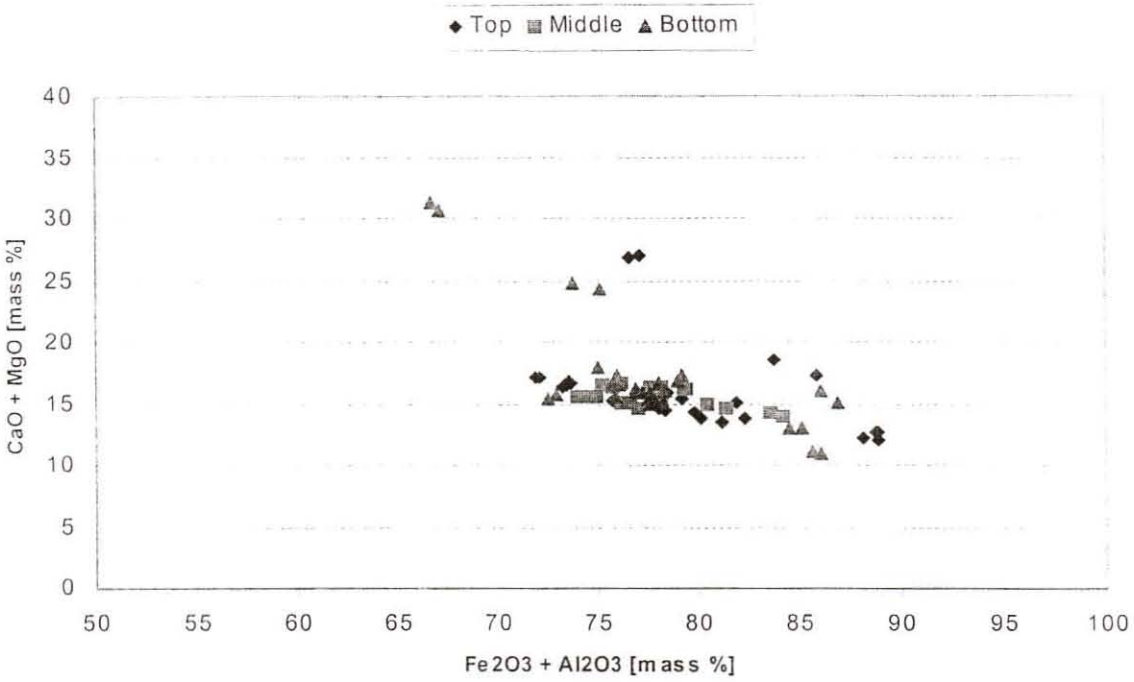

Figure 23: SFCA (Series 2)

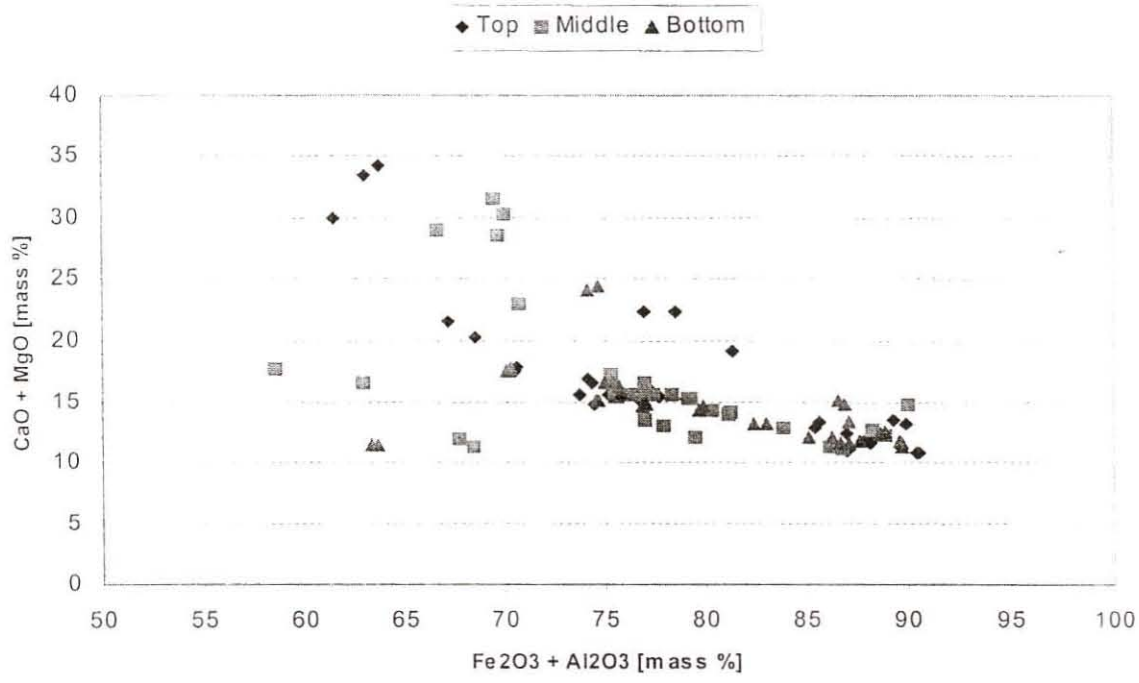

Figure 22 and **Figure 23** show the mass percentage (Fe_2O_3 + Al_2O_3) versus the mass percentage (CaO + MgO). The hypothesis tests (**APPENDIX F**) and well grouped data as shown in **Figure 22** and **Figure 23** indicates that the chemical composition of the SFCA in the different layers is almost the same. However, a few samples in series two were scattered due to the SiO_2 content higher than 10%. The most common empirical formula for SFCA is $M_{25}O_{36}$ [13]. The calculated stoichiometry (**Table 12**) of the SFCA in all the layers agrees well with the general formula $M_{25}O_{36}$ = $Ca_5,Si_2,(Fe,Al)_{18}O_{36}$. An example to show how the stoichiometry was calculated is shown in **APPENDIX G**.

Table 12: Stoichiometry of SFCA

$M_{25}O_{36} = Ca_5,Si_2,(Fe,Al)_{18}O_{36}$

	Series1: 1100mmH_2O			Series 2: 1500mmH_2O		
	Top	**Middle**	**Bottom**	**Top**	**Middle**	**Bottom**
Ca^{2+}	4.82	4.74	4.63	4.56	4.31	4.08
Si^{4+}	1.80	1.99	1.90	1.51	1.49	1.41
Fe^{3+}	17.17	16.55	16.50	17.57	17.61	17.90
Al^{3+}	1.23	1.47	1.70	1.41	1.40	1.28
M	**25.02**	**24.75**	**24.73**	**25.05**	**24.81**	**24.67**
O^{2-}	**36.00**	**36.00**	**36.00**	**36.00**	**36.00**	**36.00**

5.5.4 OTHER PHASES

The sinter contained an amorphous silicate rich glass. In some instances the glass appeared to be finely crystalline with lath like olivine crystals crystallising from the glass upon cooling of the melt.

Wustite / magnesiowustite is only present in small quantities and occurs as fine to medium grained spherical particles. The periclase is mainly present as grainy type aggregate particles consisting of abundant fine grained spherical MgO crystals and particles as shown in **Figure 25**. MnO-rich (Mn,Fe,Mg)O particles were optically observed (**Figure 24**) in some of the sinter samples. Optically this phase resembles magnetite but the individual oxide crystals display well defined twinning with strong anisotropic texture that is absent in magnetite.

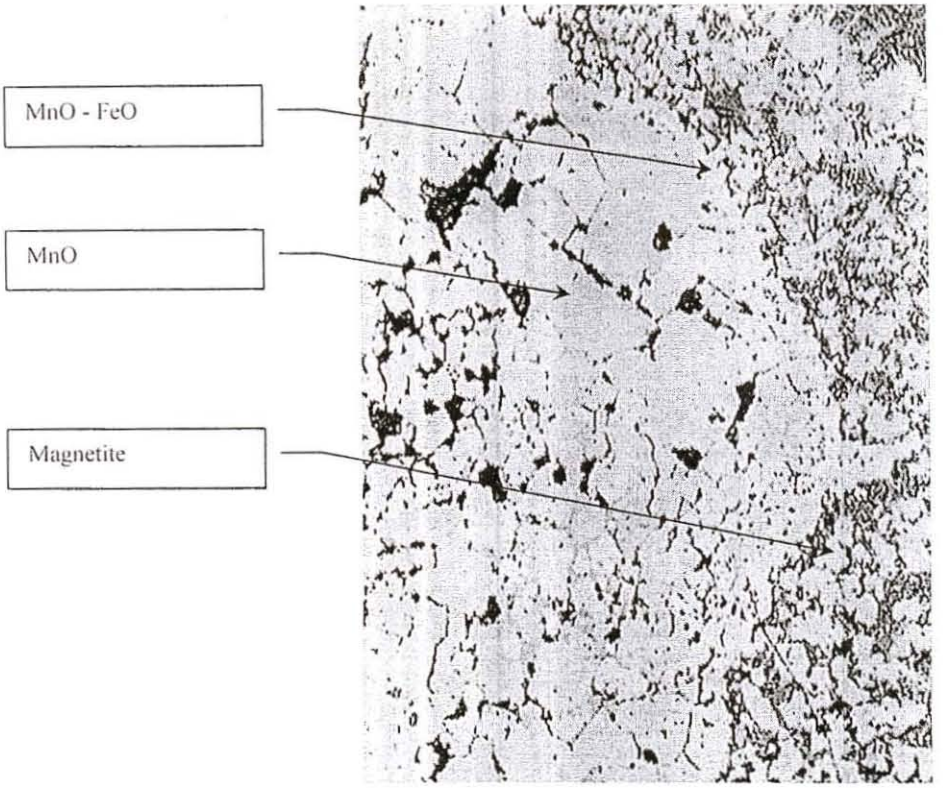

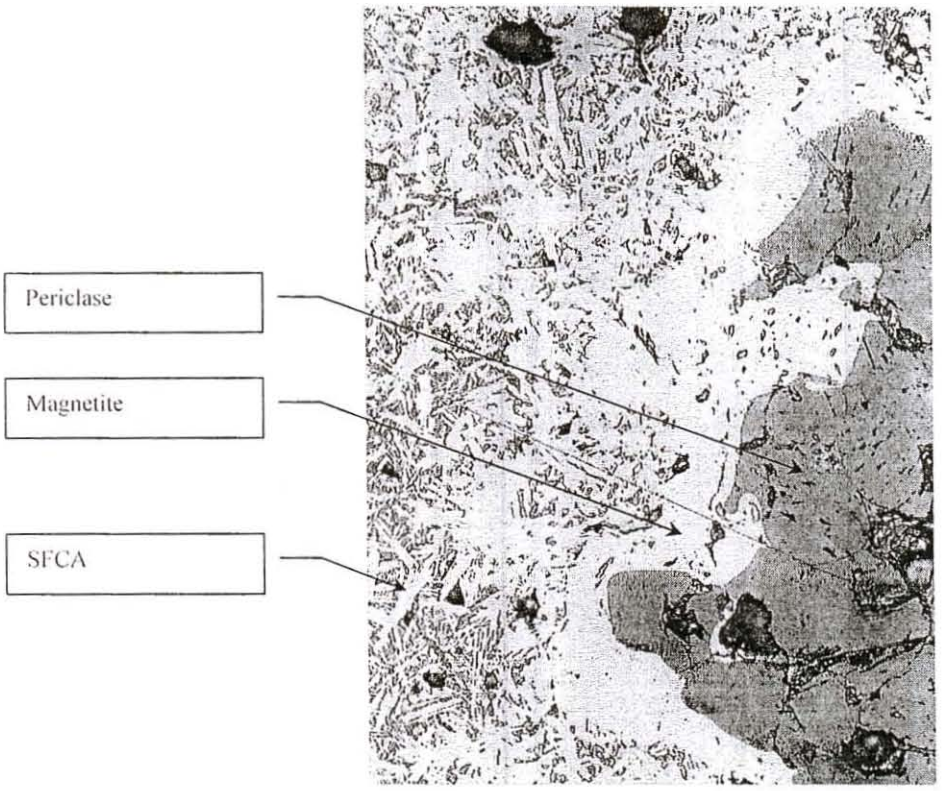

***Figures 24 and 25**: Other phases present in the sinter include manganese oxide and periclase (X 200).*

Small quantities of calcium silicate, glass, periclase, wustite and manganese occur in the sinter (**Figure 26 and 27**).

Figure 26: Other phases (Series 1)

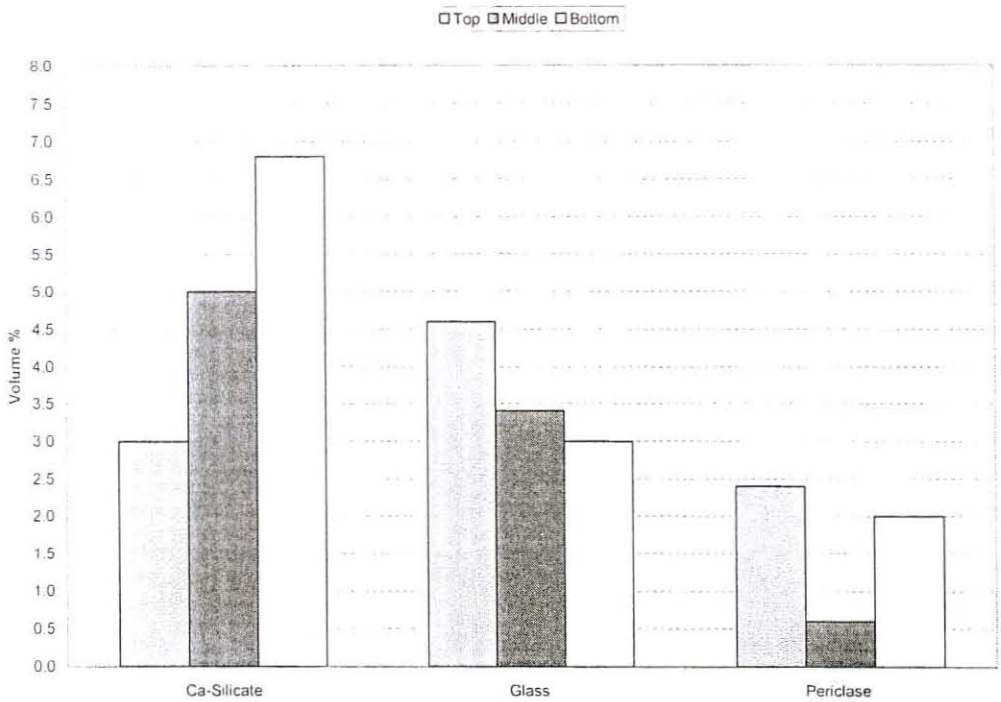

Figure 27: Other phases (Series 2)

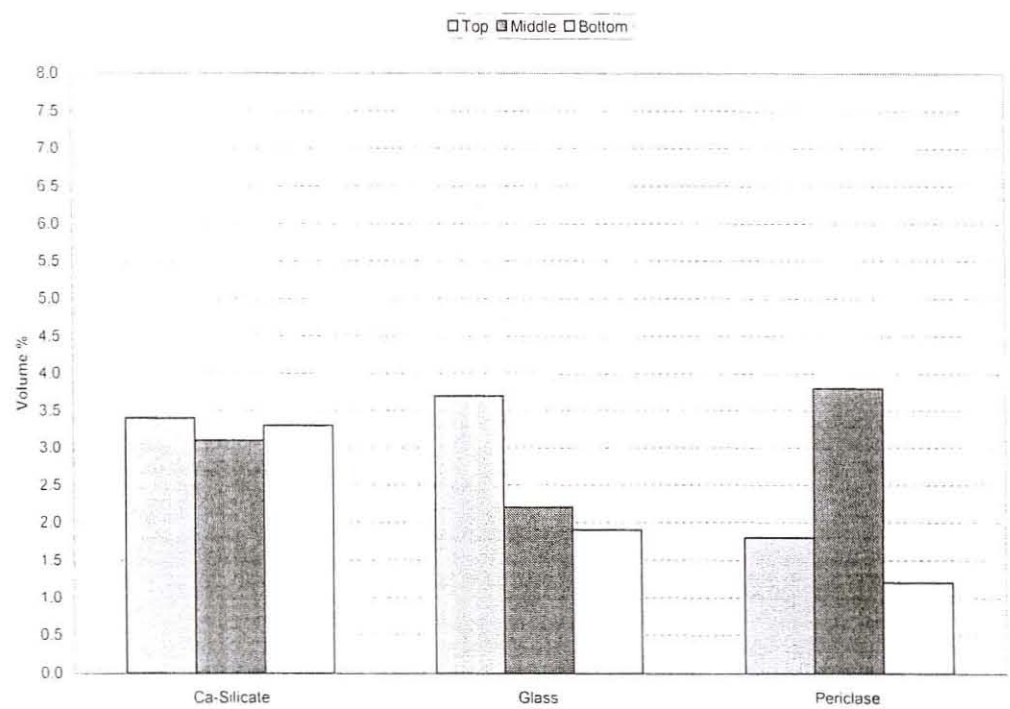

Glassy silicate, often referred to as slag phases, is formed when the melt from which primary phases have precipitated is rapidly cooled. The silicates can contain iron oxide as a substitute for calcium oxide and other impurities such as Al^{3+}, Mg^{2+} and other alkalines[3]. The calcium silicates are present as fine-grained lens shaped and/or dendritic crystals as shown in **Figure 28**. The calcium silicate is in general associated with SFCA and/or magnetite.

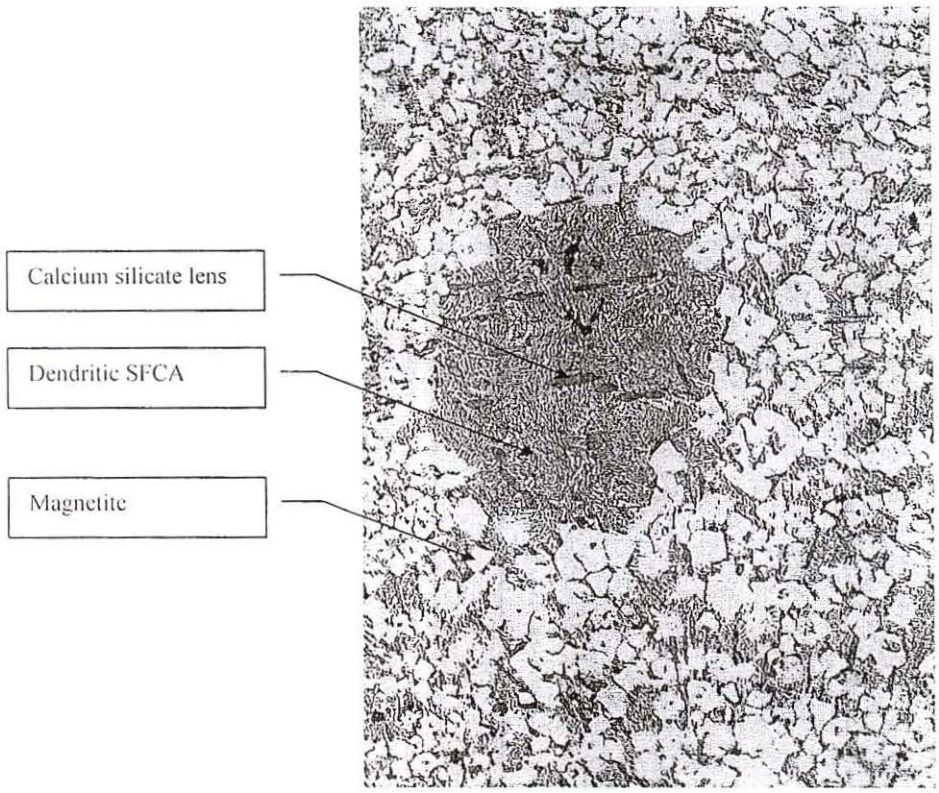

***Figure 28**: The calcium silicates are present as fine-grained lens shaped crystals. Dendritic SFCA and magnetite are embedded in a silicate rich glassy matrix (X 200).*

According to the chemical analyses data there are two different groups of calcium silicate present in the sinter produced in the sinter pot tests in both series. This difference is associated with the FeO content of the calcium silicate. In the first group the FeO content is lower than 10% while the FeO content of the second group is higher than 10% as shown in **Figure 29** and **Figure 30**.

Figure 29: Calcium silicate (Series 1)

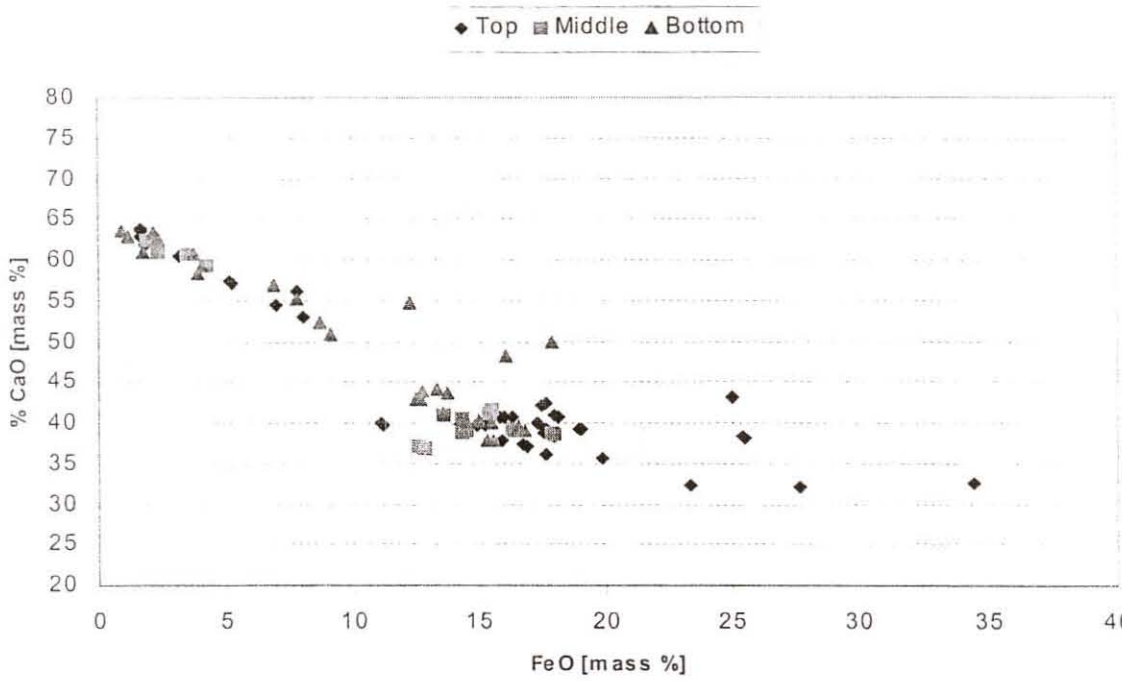

Figure 30: Calcium silicate (Series 2)

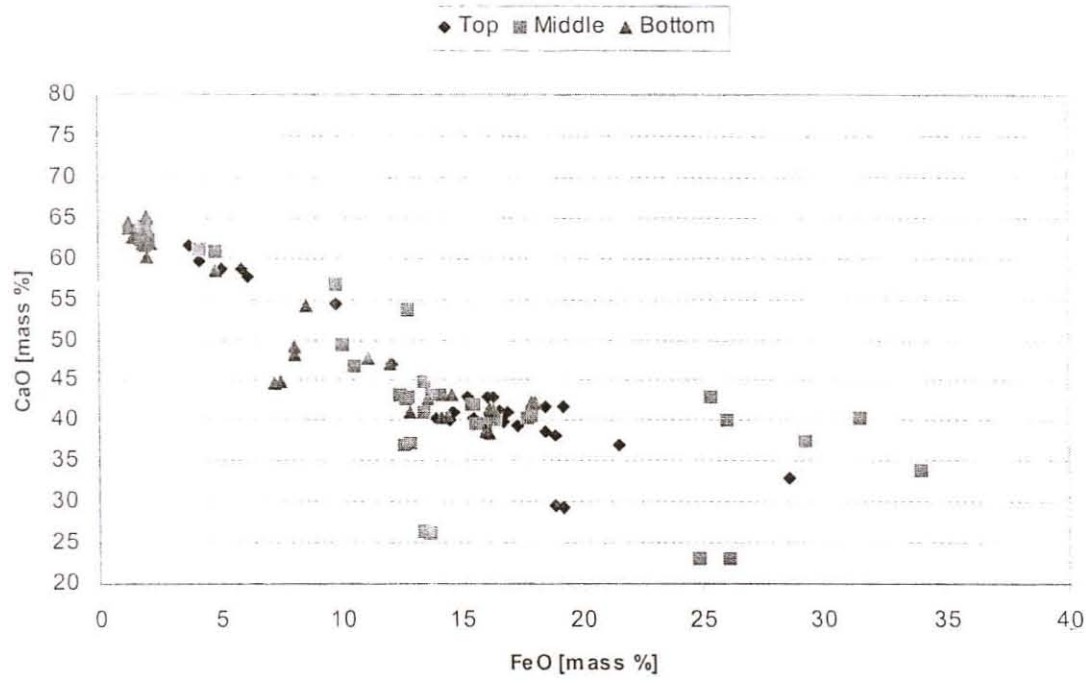

In the first group the FeO content is lower than 10% (**Table 13**). The typical CaO content is ±60% and the typical SiO_2 content is ±30%.

Table 13: Chemical analyses of the calcium silicate

(%FeO < 10%)

	Series1: 1100mmH_2O			Series 2: 1500mmH_2O		
	Top	**Middle**	**Bottom**	**Top**	**Middle**	**Bottom**
FeO	4.85	3.05	3.31	4.06	2.98	4.37
SiO_2	31.48	32.54	32.38	32.00	32.07	32.04
TiO_2	0.04	0.01	0.89	0.11	0.14	0.10
CaO	59.55	62.18	59.18	59.53	60.78	58.92
SO_3	0.07	0.04	0.43	0.10	0.10	0.15
MnO	0.05	0.08	0.05	0.08	0.05	0.07
K_2O	0.02	0.02	0.00	0.08	0.04	0.10
MgO	0.09	0.06	0.11	0.09	0.07	0.10
Al_2O_3	0.36	0.21	0.88	1.37	0.27	0.64
Na_2O	0.05	0.03	0.08	0.06	0.07	0.13
P_2O_5	1.11	0.99	0.49	1.65	2.79	0.88

Calcium oxide is replaced by iron oxide in the second group of calcium silicate. The FeO content is higher than 10% (**Table 14**). The typical CaO content changes to ±40% while the typical SiO_2 content remains at ±30%.

Table 14: Chemical analyses of the calcium silicate

(%FeO > 10%)

	Series1: 1100mmH_2O			Series 2: 1500mmH_2O		
	Top	**Middle**	**Bottom**	**Top**	**Middle**	**Bottom**
FeO	16.48	13.97	14.76	16.59	15.14	14.61
SiO_2	35.74	34.86	34.74	32.91	33.97	33.39
TiO_2	0.79	0.88	0.83	0.68	1.05	0.78
CaO	40.01	41.19	42.20	39.55	39.33	42.76
SO_3	0.10	0.08	0.18	0.16	0.08	0.12
MnO	0.18	0.24	0.13	0.21	0.28	0.16
K_2O	0.04	0.13	0.00	0.12	0.41	0.25
MgO	0.31	0.36	0.32	0.56	0.30	0.35
Al_2O_3	3.13	4.52	3.97	6.84	6.16	3.78
Na_2O	0.04	0.05	0.12	0.05	0.07	0.11
P_2O_5	0.32	0.27	0.32	0.49	0.56	0.81

5.6 CORRELATION BETWEEN PHASES AND SINTER QUALITY

Sinter quality is mainly governed by the microstructure of the sinter. Sinter is an aggregate of bonding phases, unmelted particles and pores. The bonding phases originate during the sintering process. Unmelted particles are mainly residual large ore particles and sometimes unreacted, residual flux particles.

The presence of magnetite results in the deterioration of the physical properties of the sinter. During cooling, internal tensions are developed because of the difference in shrinkage of the phases. In the case of magnetite this phenomenon is sufficient to produce cracks. Hematite is usually free of cracks, except in the areas where magnetite is precipitated. According to the literature, magnetite is the major source of crack formation and poor physical properties of the sinter[4][12].

From the results of this investigation, a strong relation between the magnetite content and sinter strength could not be found (**Figure 31**).

Figure 31: Magnetite content versus Tumbler index.

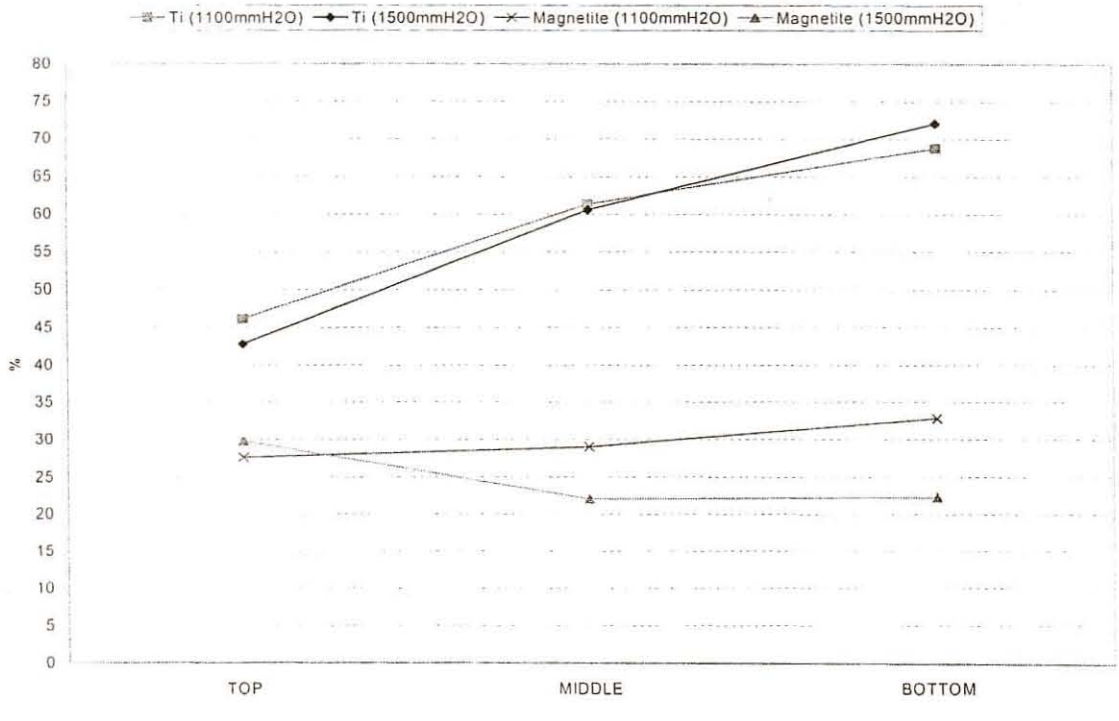

The total SFCA content increases from the top layer to the bottom layer as does the tumbler index. This correlation is shown in **Figure 32**.

Figure 32: SFCA content versus Tumbler index.

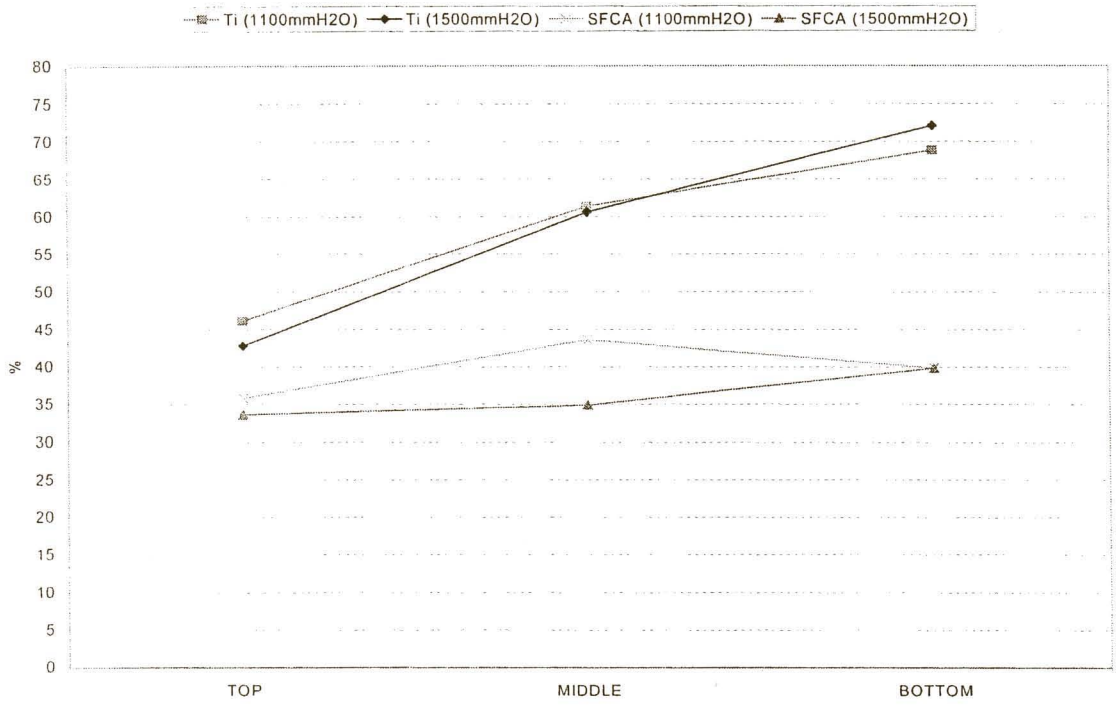

SFCA results in the improvement of the physical properties of the sinter. The bonding phases make up the majority of phases within sinter (up to 80vol%). The sinter properties are therefore strongly related to the bonding phases. The phases are formed during the sinter process at temperatures above 1100°C. SFCA is the most important bonding phase in the sinter and therefore improves the physical properties of the sinter. This is clearly illustrated when the SFCA content of the bottom layer of series one decreases the tumbler index also decreases (**Figure 32**).

The glass content of the sinter decreases from the top layer to the bottom layer while the tumbler index increases from the top layer to the bottom layer. This correlation is shown in **Figure 33**. Glass results in the deterioration of the physical properties of the sinter. The degree of breakage depends on the ease with which cracks propagate through the sinter particle. Glass is not a very strong bonding phase. Cracks will easily propagate through this phase resulting in poor physical properties.

Figure 33: Glass content versus Tumbler index.

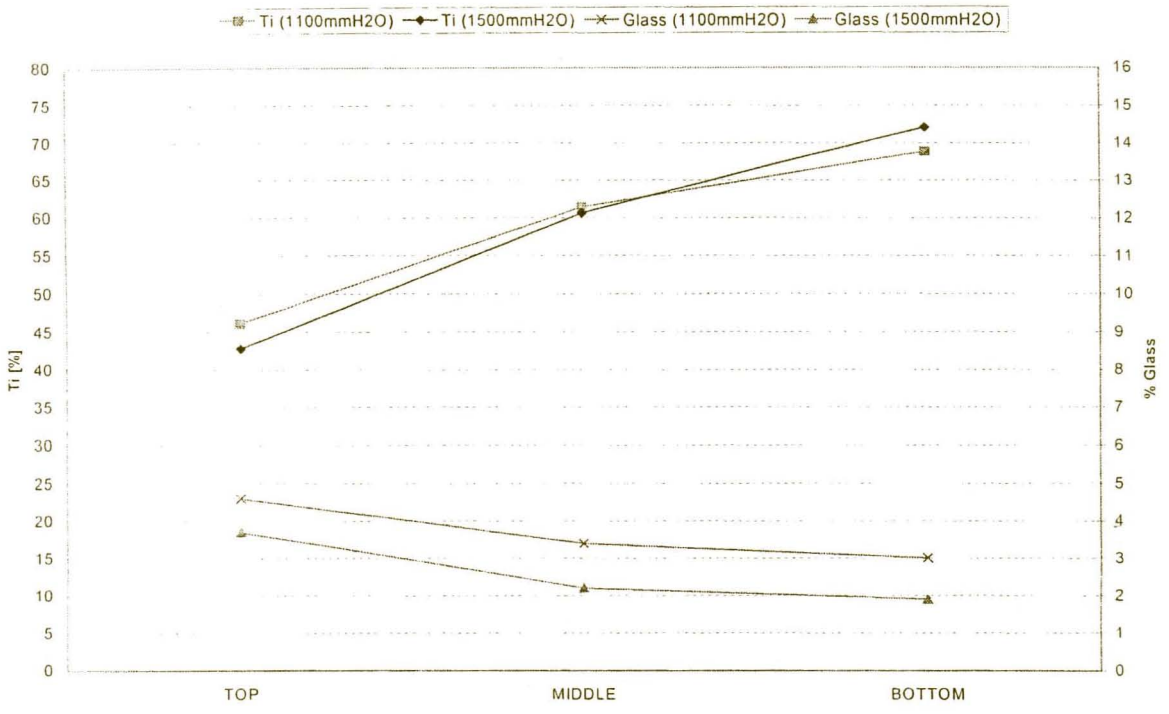

6. CONCLUSIONS

It is possible to change the temperature-time-characteristics of the sinter process by changing the airflow rate through the sinter bed. The air flow rate increased when the pressure drop over the sinter bed was increased. The rate of downward movement through the sinter bed of the combustion zone increased as a result. This was indicated by a shorter sintering time as well as different temperature profiles in the different sinter layers.

The sintering time at temperatures above 1100°C is related to the airflow rate through the sinter bed. The higher the airflow rate, the shorter the sintering time at temperatures above 1100°C. By changing the temperature-time-characteristics of the sinter process it is possible to control the sintering time at temperatures above 1100°C. The sintering time above 1100°C increased from the top layer to the bottom layer in the sinter bed.

The temperature-time-characteristics of the sinter process have a major influence on phase formation during the sinter process. The phase composition differs in each layer because each layer is subjected to different temperature-time-characteristics. This study revealed that the main constituents of the sinter were hematite, magnetite and SFCA with small quantities of calcium silicate, glass, periclase, wustite and manganosite.

The sintering time above 1100°C is one of the most important parameters to ensure that phases to enhance sinter quality are formed. At a lower airflow rate the sintering time at temperatures above 1100°C increases resulting in a higher SFCA content. The sintering time at temperatures above 1100°C increased from the top layer to the bottom layer resulting in a higher SFCA content in the middle and bottom layers.

Magnetite has a detrimental influence on the physical properties of the sinter. From the results of this investigation, a strong relation between the magnetite content and sinter strength could not be found.

SFCA results in the improvement of the physical properties of the sinter. In this study the total SFCA content increases from the top layer to the bottom layer and the physical properties improved from the top layer to the bottom layer.

Glass results in the deterioration of the physical properties of the sinter. The glass content of the sinter decreases from the top layer to the bottom layer while the physical properties improved from the top layer to the bottom layer.

In spite of the correlation found between the sinter strength and phases of the sinter in this investigation, it became clear that the phases are not the only parameter determining the sinter strength. The morphology of the sinter phases present, porosity of the sinter and coke rate may have an influence on the sinter quality and should be investigated.

In practice it is important to find an optimum between the airflow rate, sinter quality as well as production rate.